Design and Fabrication of a Lossy Ceramic Resin Absorber Based on MSLA Technology

KE JIANG, XUFENG JING*

[1]Institute of Optoelectronic Technology, China Jiliang University, Hangzhou, 310018, People's Republic of China
[2]College of Information Engineering, China Jiliang University, Hangzhou 310018, PR China
*Corresponding Author: jingxufeng@cjlu.edu.cn;

Submission: 2026-07-1; Acceptance: 2026-07-15; Publication: 2027-07-31

This paper proposes and designs an all-dielectric broadband terahertz absorber based on a high-loss ceramic-filled resin, which is fabricated using Masked Stereolithography Apparatus (MSLA) 3D printing technology to achieve efficient broadband absorption at the millimeter scale. The absorber consists of four truncated-cone resonators with gradually varying dimensions, a high-loss ceramic-filled resin dielectric substrate, and a metallic ground plane arranged in a periodic unit-cell configuration. Through the synergistic effects of multi-scale Mie resonances, gradient impedance matching, Fabry–Perot cavity resonances, and the intrinsic dielectric loss of the material, the proposed structure exhibits excellent broadband absorption performance over the frequency range of 0.22–1 THz. Numerical simulations reveal that multiple localized resonance modes are effectively coupled and merged, while magnetic dipole resonances generated by the interaction between displacement currents and induced currents on the metallic ground plane significantly improve impedance matching and enhance electromagnetic energy localization. The absorber samples were successfully fabricated using MSLA photocuring 3D printing technology and experimentally characterized by a terahertz time-domain spectroscopy (THz-TDS) system to evaluate both the electromagnetic properties of the material and the absorption performance of the device. Experimental results demonstrate that the absorber achieves near-unity absorption within the frequency range of 0.2 – 1.8 THz and maintains excellent polarization stability. This work provides a feasible route for the low-cost and high-precision fabrication of all-dielectric terahertz absorbers and offers significant potential for applications in terahertz electromagnetic wave manipulation and control.

Keywords: All-dielectric absorber; Terahertz absorber; Broadband absorption; MSLA 3D printing; Ceramic-filled resin.

1. Introduction

In this chapter, a broadband all-dielectric metamaterial absorber operating in the terahertz frequency range is proposed. The designed structure simultaneously considers electromagnetic absorption performance and the practical manufacturability afforded by advanced additive manufacturing technologies. Conventional terahertz metasurface absorbers generally rely on subwavelength metallic resonators with feature sizes at the sub-100 μm scale, resulting in complex fabrication processes, high manufacturing costs, and limited scalability for large-area production[1-4]. To overcome these limitations, an all-dielectric absorption scheme based on multiscale dielectric resonances is adopted in this work. Combined with high-precision Masked Stereolithography Apparatus (MSLA) three-dimensional printing technology, broadband absorption is achieved using a millimeter-scale structure with excellent fabrication feasibility.

Traditional metallic metamaterial absorbers achieve electromagnetic wave attenuation primarily through metallic resonant structures[4-7]. However, their performance in the terahertz regime is often constrained by Ohmic losses, skin effects, and inherently narrow absorption bandwidths. In contrast, all-dielectric metamaterial absorbers manipulate electromagnetic waves through displacement currents and Mie resonances generated within dielectric materials. Such structures exhibit several advantages, including reduced conductive losses, superior angular stability, and compatibility with three-dimensional integration, making them an increasingly attractive solution for terahertz absorption applications.

At present, most reported all-dielectric terahertz absorbers are based on single-resonance configurations, resulting in relatively narrow absorption bandwidths that are insufficient for broadband applications[7-10]. To broaden the operational bandwidth, various design strategies have been proposed, including multiscale resonant structures, gradient impedance matching, and multilayer coupling mechanisms. Among these approaches, gradient structures effectively mitigate impedance mismatch between free space and dielectric media, while resonators with different characteristic dimensions can excite multiple localized resonance modes at distinct frequencies. The superposition and coupling of these resonances lead to the formation of multiple absorption peaks, thereby enhancing the overall broadband absorption performance.

Meanwhile, the rapid development of additive manufacturing technologies has provided new opportunities for the fabrication of terahertz metamaterial devices. In particular, Masked Stereolithography Apparatus

(MSLA), which is based on LCD-assisted photopolymerization, has attracted increasing attention due to its high fabrication efficiency, low production cost, and capability to manufacture complex three-dimensional geometries. Consequently, MSLA has gradually been introduced into the fabrication of terahertz metamaterials and functional electromagnetic devices. Nevertheless, research on broadband all-dielectric terahertz absorbers fabricated by MSLA remains relatively limited, especially for structures employing high-loss ceramic-filled resin materials, for which systematic investigations are still scarce.

Motivated by these considerations, a broadband all-dielectric terahertz absorber based on a high-loss ceramic-filled resin is proposed in this work. The absorber consists of four truncated-cone resonators with different dimensions, a dielectric substrate, and a metallic ground plane. Through the synergistic effects of multiscale Mie resonances, gradient impedance matching, Fabry – Perot cavity resonances, and the intrinsic dielectric loss of the material, efficient broadband absorption is achieved over a wide frequency range. Furthermore, to ensure practical manufacturability, the structural parameters were optimized according to the characteristics and resolution limits of the MSLA printing process. Numerical simulation results demonstrate that the proposed absorber exhibits excellent broadband absorption performance within the frequency range of 0.2-1.0 THz, while maintaining favorable polarization insensitivity and angular stability.

2. The structural design

The proposed all-dielectric terahertz absorber consists of four gradient truncated-cone resonators, a high-loss ceramic-filled resin dielectric substrate, and a metallic ground plane. The absorber adopts a periodic unit-cell array configuration, in which broadband absorption of terahertz electromagnetic waves is achieved through the construction of multi-scale gradient resonant structures on the dielectric surface.

To simultaneously satisfy the operational requirements in the terahertz frequency range and the manufacturability constraints of the MSLA printing process, the structural dimensions were carefully optimized. Considering that LCD-based photopolymerization printing with highly ceramic-filled resin is susceptible to light scattering and over-curing effects, excessively small structural features are prone to edge collapse, tip adhesion, and dimensional distortion. Therefore, millimeter-scale gradient truncated-cone resonators were employed in this work to improve fabrication accuracy and ensure consistency between simulations and experiments. Furthermore, compared with sharp conical structures, truncated cones retain a finite top platform, which effectively alleviates tip deformation during printing and enhances structural stability.

The dielectric substrate is fabricated from a high-loss ceramic-filled resin with a relative permittivity of approximately 3 and a loss tangent of about 0.05. Compared with conventional low-loss dielectric materials, this material exhibits stronger electromagnetic energy dissipation capability. When incident electromagnetic waves propagate into the absorber, a substantial amount of electromagnetic energy is confined within the dielectric region under the enhancement of localized resonances and is subsequently converted into thermal energy through dipolar polarization loss, interfacial polarization loss, and conductive loss, thereby further improving the absorption performance. The metallic ground plane is made of copper, whose thickness is much greater than the skin depth at terahertz frequencies; therefore, the transmission coefficient can be considered negligible.

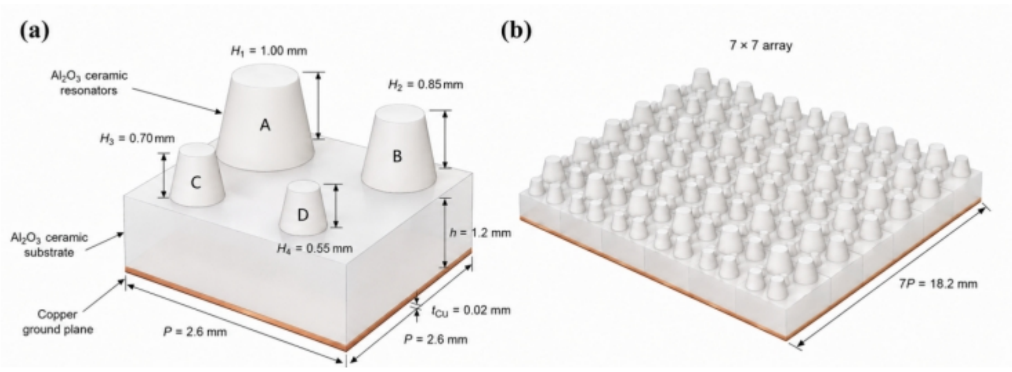

Fig. 1. Schematic diagram of metamaterial absorber: (a) Unit structure schematic diagram; (b) Array structure schematic diagram

As illustrated in Fig. 1(a), the absorber consists of an air layer, a gradient truncated-cone resonator layer, a high-loss dielectric substrate, and a metallic ground plane arranged sequentially from top to bottom. The resonator layer comprises four truncated-cone structures with different dimensions arranged in a symmetric 2 × 2 configuration. The fabricated array sample used for subsequent measurements is shown in Fig.1(b). Truncated-cone resonators of different sizes can excite localized Mie resonances at different frequencies, thereby generating multiple absorption peaks. Meanwhile, the gradient resonator configuration provides a smooth impedance transition between air and the dielectric medium, reducing interface reflections and achieving gradient impedance matching. The metallic ground plane suppresses electromagnetic wave transmission and confines more incident energy within the dielectric region, thereby enhancing the overall absorption performance.

The unit-cell period of the absorber is set to 2.6 mm, while the thickness of the dielectric substrate is 1.2 mm. The four truncated-cone resonators are arranged in a centrosymmetric configuration with a center-to-center spacing of 1.10 mm. This arrangement effectively enhances the near-field coupling interactions among adjacent resonators and improves the polarization stability of the structure.

Under normal incidence of electromagnetic waves, the truncated-cone resonators with different dimensions excite electric-dipole and magnetic-dipole resonances at distinct frequencies. The resulting localized resonance modes overlap and couple with one another, leading to the formation of a continuous broadband absorption response. The detailed geometrical parameters of the proposed absorber are summarized in Table 1.

Resonator Number	Bottom diameter (mm)	Top diameter (mm)	Height (mm)	Main resonant frequency band (THZ)
A	1.2	0.72	1	0.22-0.35
B	1	0.6	0.85	0.32-0.48
C	0.82	0.48	0.7	0.45-0.65
D	0.66	0.38	0.55	0.60-0.85

Table 1. Comparison of Multiband Characteristics of Tunable Metasurface Absorbers

3.Simulation results and mechanism analysis of the absorber

A.Absorption performance and impedance matching analysis

To evaluate the absorption performance of the proposed all-dielectric absorber, full-wave electromagnetic simulations were carried out using CST Microwave Studio. The simulations were performed with the Frequency Domain Solver. Periodic boundary conditions were applied along the X- and Y-directions, while open boundary conditions were imposed along the Z-direction to emulate an infinite periodic array. A plane electromagnetic wave was normally incident along the negative Z-direction, with the electric field polarized along the X-axis and the magnetic field polarized along the Y-axis. The simulation frequency range was set from 0.1 to 1.0 THz.

Fig.2(a) and 2(b) present the simulated absorption, reflection, and transmission spectra of the absorber within the frequency range of 0.1–1.0 THz. Owing to the presence of the metallic ground plane, the transmission can be considered negligible. As observed from the results, the proposed absorber exhibits excellent absorption performance over a broad frequency range from 0.22 to 0.85 THz, with the absorptance exceeding 90% at multiple resonance frequencies, thereby forming a pronounced broadband absorption band. Compared with conventional single-resonance all-dielectric absorbers, the proposed design achieves a significantly enhanced absorption bandwidth.

The broadband absorption behavior primarily originates from the multimode coupling effect induced by the multi-scale gradient truncated-cone resonators. The four resonators with different dimensions excite localized Mie resonances at distinct frequencies, and the corresponding resonance modes overlap and merge to form a continuous broadband absorption response. In addition, the gradient truncated-cone configuration provides a smooth impedance transition between free space and the dielectric medium, thereby reducing interface reflections and facilitating the penetration of incident electromagnetic waves into the absorber.

Meanwhile, the high-loss ceramic-filled resin possesses a relatively large loss tangent. Once electromagnetic waves enter the dielectric region, a considerable amount of electromagnetic energy is confined within the structure due to the enhancement of localized resonances and is subsequently dissipated as heat through dielectric losses. This energy conversion mechanism further contributes to the improvement of the absorption efficiency.

To gain deeper insight into the absorption mechanism, the normalized effective impedance of the absorber was investigated. According to the effective medium theory, the metamaterial absorber can be regarded as an equivalent homogeneous medium, and its normalized impedance can be retrieved from the scattering parameters (S-parameters), as shown in Fig.2(c) and (d). When the effective impedance of the structure approaches that of free space, incident electromagnetic waves can efficiently enter the absorber, thereby suppressing reflection and enhancing absorption performance.

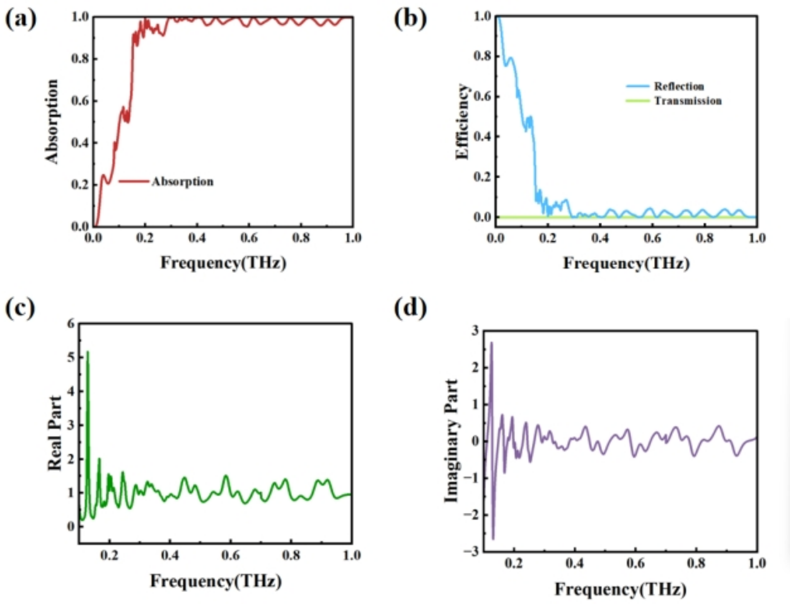

Fig. 2.Schematic diagram of metamaterial performance: (a) Absorption rate; (b) Reflection and transmission rates of the absorber; (c) Real part of impedance matching; (d) Imaginary part of impedance matching

B.Electric field distribution analysis

To investigate the localization characteristics of electromagnetic energy within the absorber, the electric-field distributions at four representative frequencies, namely 0.2 THz, 0.4 THz, 0.6 THz, and 0.8 THz, were analyzed, as shown in Fig. 3.

It can be observed that the regions of enhanced electric field are primarily concentrated at the top surfaces and edge regions of the truncated-cone resonators at different frequencies. This indicates that, after the incident electromagnetic waves enter the structure, significant electric-field localization occurs at the dielectric–air interfaces. Such field enhancement originates from the accumulation of displacement currents caused by the abrupt permittivity discontinuity, resulting in effective confinement of electromagnetic energy in the vicinity of the resonators.

At 0.2 THz, the strongest electric-field concentration is observed around the top and sidewall regions of the largest truncated-cone resonator, while the responses of the remaining resonators are relatively weak. This phenomenon indicates that low-frequency electromagnetic waves preferentially couple with the resonator possessing the largest dimensions. Consequently, electromagnetic energy is mainly stored within the largest resonator, giving rise to a pronounced localized energy-storage effect.

When the frequency increases to 0.4 THz, significant electric-field enhancement begins to appear in the medium-sized truncated-cone resonators. The high-field regions gradually expand from a single resonator to multiple resonators, indicating that resonators of different sizes simultaneously participate in the electromagnetic response. Moreover, the spatial extent of the localized field distribution increases noticeably, suggesting the emergence of near-field coupling interactions among adjacent resonators.

As the frequency further increases to 0.6 THz and 0.8 THz, the regions of enhanced electric field gradually shift toward the smaller truncated-cone resonators, while localized hotspots are simultaneously formed along the edges of multiple resonators. This behavior reveals a pronounced size-selective resonance characteristic within the structure, whereby resonators with different dimensions are responsible for resonance excitation within different frequency ranges. As multiple resonance modes overlap and interact in the frequency domain, a continuous broadband absorption response is ultimately established.

Overall, the results demonstrate that the proposed gradient truncated-cone structure enables frequency-dependent spatial redistribution of electromagnetic energy. Resonators of different scales sequentially contribute to electromagnetic energy capture and storage over distinct frequency ranges, thereby maintaining strong localized field enhancement across a broad spectrum. This mechanism provides a fundamental basis for achieving broadband terahertz absorption.

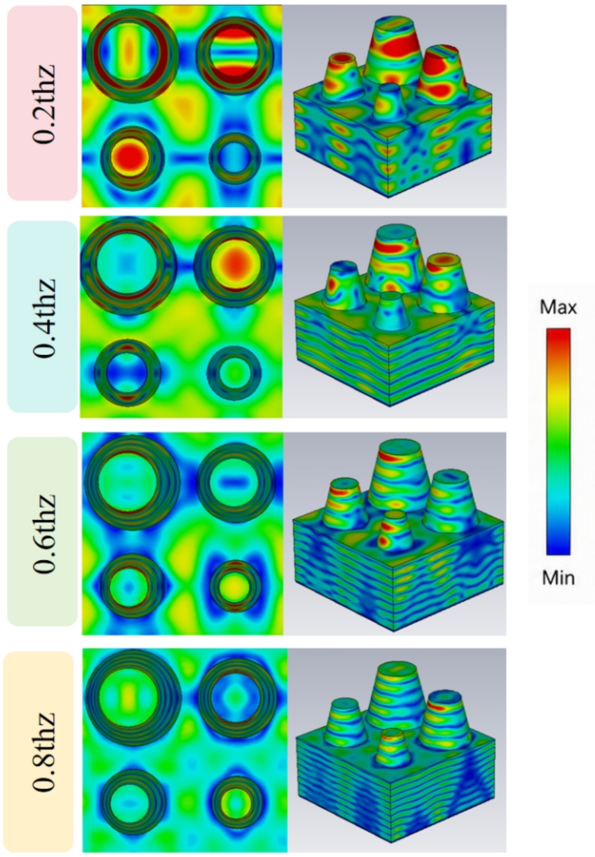

Fig. 3.electric field distribution

C.Magnetic field and current distribution analysis

To further elucidate the magnetic response characteristics of the proposed absorber, the magnetic-field distributions at 0.2 THz, 0.4 THz, 0.6 THz, and 0.8 THz were analyzed, as shown in Fig. 4. Unlike the electric-field distributions, which primarily indicate the locations of electromagnetic energy storage, the magnetic-field distributions directly reveal the formation and evolution of magnetic resonance modes within the structure. It can be observed that, throughout the major absorption band, the magnetic energy is predominantly localized inside the truncated-cone resonators and within the dielectric region between the resonators and the metallic ground plane. Furthermore, the magnetic-field distribution exhibits pronounced spatial migration as the frequency increases.

At 0.2 THz, the magnetic field is mainly concentrated within the largest truncated-cone resonator, indicating that the magnetic resonance mode is first excited in the resonator with the largest dimensions under low-frequency excitation. As the frequency increases to 0.4 THz, significant magnetic-field enhancement emerges within the medium-sized resonators. The magnetic energy gradually extends from a single resonator to multiple resonators, suggesting the onset of a multimode cooperative resonance regime.

When the frequency reaches 0.6 THz, enhanced magnetic fields are observed in all resonators to varying degrees, demonstrating that resonators of different scales simultaneously participate in the magnetic resonance process. At this stage, multiple localized magnetic hotspots are formed throughout the structure, significantly increasing the electromagnetic energy residence time and strengthening the coupling efficiency between the incident waves and the resonant elements.

As the frequency further increases to approximately 0.8 THz, the magnetic hotspots progressively shift toward the smaller resonators, while the larger resonators continue to maintain a certain level of magnetic response. This phenomenon indicates the existence of persistent electromagnetic coupling among resonators of different scales. Through the collective contribution of these resonators, strong magnetic resonance characteristics can be sustained over a broad frequency range, thereby facilitating the realization of broadband absorption.

From the perspective of the underlying physical mechanism, the localized magnetic-field enhancement originates from the circulating displacement-current loops established within the dielectric resonators. When the displacement currents form closed-loop paths inside the resonators, pronounced magnetic dipole resonances are excited, leading to an increase in the effective permeability of the structure. Since both the effective permeability and effective permittivity can be simultaneously engineered, the proposed absorber is capable of achieving impedance matching with free space over a broad frequency range, thereby suppressing reflection and enhancing absorption efficiency. Therefore, the magnetic-field distributions demonstrate that the multi-scale truncated-cone resonators not only enable broadband localization of electromagnetic energy but also continuously regulate the effective electromagnetic parameters of the structure through sustained magnetic dipole resonances. This mechanism constitutes one of the key factors responsible for the observed broadband high-absorption performance.

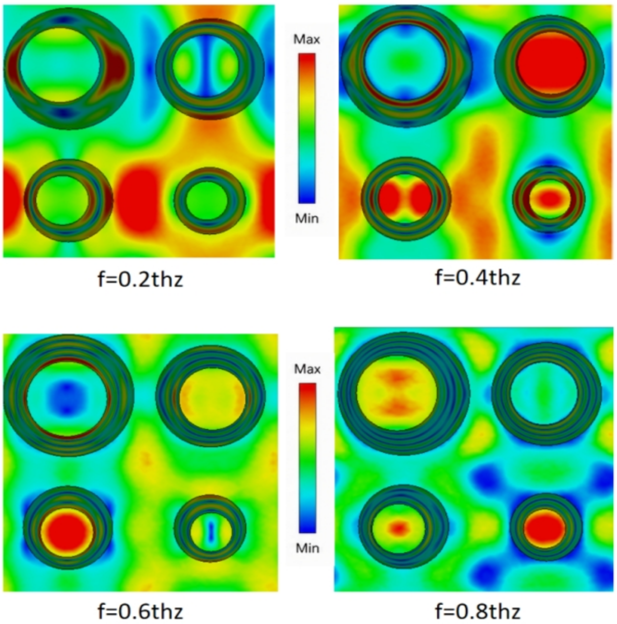

Fig.4. Magnetic field distribution

To further verify the formation mechanism of the magnetic resonances, the surface current distributions on the metallic ground plane were investigated, as shown in Fig.5 It should be noted that the high-loss ceramic-filled resin is a dielectric material and therefore contains no free electrons. Consequently, the surface currents presented in the figure do not originate from the dielectric resonators themselves but rather from the induced currents on the metallic ground plane. When the incident electromagnetic wave excites oscillating displacement currents within the truncated-cone resonators, corresponding induced currents are generated on the metallic ground plane, forming complete current-loop configurations together with the displacement currents.

At 0.2 THz, the induced currents are mainly concentrated in the regions corresponding to the two smaller resonators, indicating that electromagnetic energy can already be efficiently transferred through dielectric coupling to the metallic ground plane, thereby generating localized current responses. As the frequency increases to 0.4 THz, the induced currents become significantly stronger and exhibit relatively well-defined directional distributions in certain regions, suggesting enhanced coupling between the displacement currents and the induced currents.

When the frequency reaches 0.6 THz, the current distribution gradually evolves from localized excitation to a multi-region cooperative response. Distinct induced currents appear beneath multiple resonators, indicating that the absorber has entered a multimode coupling regime. Under this condition, electromagnetic energy can be effectively transferred and exchanged among resonators of different scales, which contributes to the broadening of the absorption bandwidth.

At 0.8 THz, pronounced current responses are observed beneath both the larger and smaller resonators, demonstrating that strong electromagnetic coupling is maintained among resonators of different dimensions. As a result, resonators with multiple characteristic scales collectively participate in the high-frequency absorption process, further supporting the broadband absorption behavior of the proposed structure.

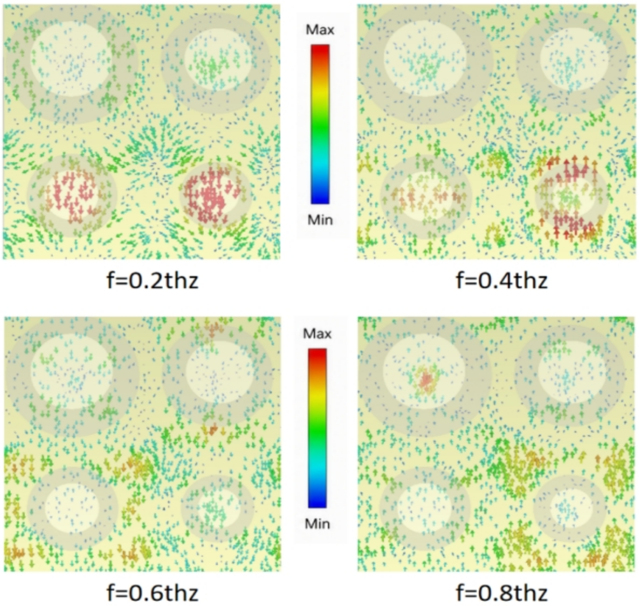

Fig.5. Current distribution

By correlating the surface current distributions with the magnetic-field distributions, it can be observed that the regions exhibiting the strongest induced currents correspond closely to the locations of enhanced magnetic fields. According to Ampère's circuital law, the displacement currents within the dielectric resonators and the induced currents on the metallic ground plane form antiparallel closed current loops. These current loops generate strong localized magnetic fields and subsequently excite pronounced magnetic dipole resonances. Therefore, the surface current distributions provide direct evidence, from the perspective of current dynamics, for the magnetic resonance phenomena observed in the magnetic-field distributions. These results further confirm the proposed absorption mechanism and provide important physical evidence for the broadband electromagnetic absorption behavior of the designed structure.

D.Absorption mechanism analysis

To further elucidate the broadband absorption mechanism of the proposed all-dielectric absorber, a comprehensive analysis was conducted by correlating the absorption spectra, impedance-matching characteristics, electric-field distributions, magnetic-field distributions, and surface current distributions.

The results indicate that the excellent absorption performance of the proposed structure does not originate from a single resonance mode. Instead, it results from the synergistic interaction of gradient impedance matching, multi-scale Mie resonances, magnetic dipole resonances, Fabry–Perot cavity resonances, and the intrinsic dielectric losses of the material.

First, from a geometrical perspective, the four truncated-cone resonators form a typical gradient-impedance structure. Owing to the gradual variation in resonator diameter along the vertical direction, the effective impedance can continuously transition from free space to the dielectric medium, thereby reducing electromagnetic-wave reflection caused by abrupt impedance discontinuities at the interface. As a result, a larger portion of the incident terahertz energy can penetrate into the absorber, providing favorable conditions for subsequent resonant absorption processes.

Second, resonators with different dimensions support localized resonance modes within different frequency ranges. As the frequency increases, resonators of different scales are sequentially excited, giving rise to a pronounced size-selective electromagnetic response. The electric-field distributions demonstrate that electromagnetic energy is localized around resonators of different sizes at different frequencies, forming multiple localized energy-storage regions within the structure. These observations indicate the existence of several distinct yet spectrally adjacent resonance modes. Through spectral overlap and mutual coupling, these resonance modes merge into a continuous absorption band, ultimately resulting in broadband absorption behavior.

Meanwhile, the localized electric fields generate circulating displacement currents within the dielectric resonators, leading to significant magnetic-field enhancement. The magnetic-field distributions reveal that magnetic energy is predominantly concentrated in the dielectric region between the truncated-cone resonators and the metallic ground plane throughout the primary absorption band, indicating the formation of stable magnetic dipole resonance modes. These magnetic dipole resonances effectively regulate the effective permeability of the absorber, which, together with the effective permittivity, enables impedance matching with free space. When the input impedance of the structure approaches that of free space, surface reflections are substantially suppressed, allowing most of the incident electromagnetic energy to enter the absorber and undergo further dissipation.

Furthermore, the surface current analysis provides additional insight into the physical origin of the magnetic dipole resonances. The displacement currents inside the dielectric resonators and the induced currents on the metallic ground plane flow in opposite directions and collectively form closed current-loop configurations. According to Ampère's circuital law, these current loops generate strong localized magnetic fields and consequently excite magnetic dipole resonances. Therefore, the surface current distributions and magnetic-field distributions mutually corroborate each other, confirming the crucial role of magnetic resonances in the broadband absorption process.

It is also noteworthy that the dielectric layer and the metallic ground plane together form a typical Fabry–Perot resonant cavity. After entering the dielectric region, the incident electromagnetic waves undergo multiple reflections between the dielectric layer and the metallic ground plane, resulting in standing-wave resonance. This process effectively increases both the propagation path length and the residence time of electromagnetic waves within the absorber. In particular, it enhances electromagnetic energy confinement at lower frequencies and contributes significantly to the improvement of low-frequency absorption performance.

Finally, the electromagnetic energy confined within the structure is primarily dissipated as heat through the high-loss ceramic-filled resin. Owing to its relatively large dielectric loss, polarization relaxation loss, interfacial polarization loss, and conductive loss continuously consume the localized electromagnetic energy. The energy accumulated in the regions of enhanced electric field is ultimately converted into thermal energy within the dielectric material, thereby achieving efficient electromagnetic absorption.

In summary, the broadband absorption mechanism of the proposed absorber can be described as follows. The gradient truncated-cone structure first establishes a smooth impedance transition between free space and the dielectric medium, thereby reducing reflection losses. Subsequently, multi-scale resonators sequentially excite localized Mie resonances and confine electromagnetic energy within the structure. The interaction between displacement currents and induced currents on the metallic ground plane forms closed current loops, which excite magnetic dipole resonances and further improve impedance matching. Simultaneously, Fabry–Perot cavity resonances increase the residence time of electromagnetic waves within the absorber. The localized electromagnetic energy is then efficiently dissipated through the intrinsic losses of the high-loss ceramic-filled resin. Through the combined and cooperative effects of these mechanisms, the proposed structure achieves efficient broadband absorption over the frequency range of 0.2–1 THz.

4. Experiment

A.Absorber production

To verify the practical manufacturability of the proposed all-dielectric terahertz absorber, the samples were fabricated using LCD-based photocuring 3D printing technology based on Masked Stereolithography Apparatus (MSLA). MSLA technology selectively cures liquid photosensitive resin through digitally controlled ultraviolet exposure, enabling the layer-by-layer fabrication of complex three-dimensional structures. Compared with conventional machining methods, this technique offers several advantages, including high fabrication accuracy, high manufacturing efficiency, excellent surface quality, and strong adaptability to complex geometries. These characteristics make it particularly suitable for the rapid prototyping of metamaterials and terahertz devices.

Fig. 6 presents the MSLA photocuring 3D printer (3DSZ-DL1, Digital Manufacturing Technology Co., Ltd.) used in this work. The printer employs LCD mask-based exposure technology and provides high printing precision and fabrication efficiency, thereby meeting the manufacturing requirements of the complex microstructures involved in metamaterial absorbers. The photosensitive resin used in the experiments was MD8100, which exhibits excellent photocuring characteristics, good flowability, and high dimensional stability. Under ultraviolet irradiation, the resin rapidly undergoes polymerization and forms stable solid structures. In addition, the recommended initial printing parameters adopted in this study are summarized in Table 2. These parameters may be appropriately adjusted according to specific fabrication conditions and experimental requirements.

Table 2. MLSA Photopolymer Resin Printing Parameters

Parameter	**Setting**	**Unit / Notes**
Layer thickness	0.05	mm
Bottom layer count	5	layers
Normal exposure time	2	s
Bottom exposure time	50	s
Transition layer count	5	layers
Transition type	Linear	-
Transition layer time increment	4.53	s

Printing wait mode	Static	-
Rest time before lifting	4.000	s
Rest time after lifting	0.000	s
Rest time after retracting	2.000	s
Bottom lift distance	5 + 3	mm; two-stage setting
Normal lift distance	5 + 3	mm; two-stage setting
Bottom retract distance	5 + 3	mm; two-stage setting
Normal retract distance	5 + 3	mm; two-stage setting
Bottom lift speed	35 & 150	mm/min; two-stage setting
Normal lift speed	35 & 150	mm/min; two-stage setting
Bottom retract speed	150 & 60	mm/min; two-stage setting
Normal retract speed	150 & 60	mm/min; two-stage setting

Fig. 6 illustrates the fabrication process of the proposed absorber samples.The overall procedure mainly consists of three stages: model construction and slicing, MSLA-based 3D printing, and post-processing.First, according to the optimized structural parameters obtained in Chapter 2, a three-dimensional array model of the absorber was established using computer-aided design (CAD) software. The model consists of a high-loss ceramic-filled resin substrate and four gradient truncated-cone resonators with different dimensions arranged periodically. After the completion of the three-dimensional design, the model was exported as an STL file and imported into slicing software for preprocessing.

The slicing software automatically performs model repair, printing-orientation optimization, and support-structure generation. Subsequently, the three-dimensional model is discretized into a series of two-dimensional slices according to the predefined layer thickness. During the slicing process, several key printing parameters must be specified, including layer thickness, exposure time, bottom-layer exposure time, and lifting speed. Among these parameters, the layer thickness directly affects the surface quality and dimensional accuracy of the fabricated structure, whereas the exposure settings determine the curing depth of the resin and the bonding quality between adjacent layers.

After the slicing process is completed, a printer-compatible file is generated and transferred to the MSLA printing system for fabrication.

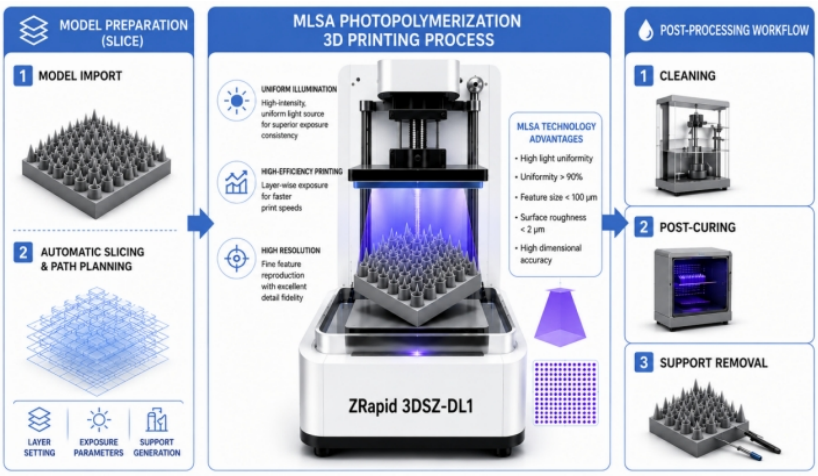

Fig.6. The process of making a wave absorber

The absorber samples were fabricated using a 3DSZ-DL1 photocuring 3D printer based on Masked Stereolithography Apparatus (MSLA) technology. Fig.7 illustrates the operating principle of the printing system and the layer-by-layer fabrication process. The system mainly consists of a UV light source, an optical homogenization module, an LCD masking screen, a transparent fluorinated ethylene propylene (FEP) release film, a resin vat, and a Z-axis motion platform.

In the printing process, ultraviolet light with a wavelength range of 365–405 nm is emitted by a UV LED array and subsequently passes through the optical homogenization system to generate a uniform illumination field. The homogenized light then reaches the LCD masking screen, where the ultraviolet light is selectively transmitted according to the two-dimensional slice image corresponding to the current printing layer. As a result, only the designated regions are exposed, thereby generating the exposure pattern required for the fabrication of the current layer.

Once exposure begins, the transmitted ultraviolet light passes through the transparent FEP release film and irradiates the surface of the liquid photosensitive resin. Under the action of the photoinitiator, free-radical polymerization is triggered within the exposed regions, causing the resin to transform from a liquid state into a solid state and thereby forming the two-dimensional cross-sectional geometry of the current layer.

After the completion of a single exposure cycle, the build platform moves upward along the Z-axis by a predefined layer thickness, allowing fresh resin to flow into the gap between the cured layer and the FEP film. Subsequently, the next layer is exposed and cured, with the newly solidified layer bonding to the previously formed layer. Through the repeated sequence of exposure, curing, platform lifting, and resin replenishment, the complete three-dimensional structure is gradually constructed in a layer-by-layer manner.

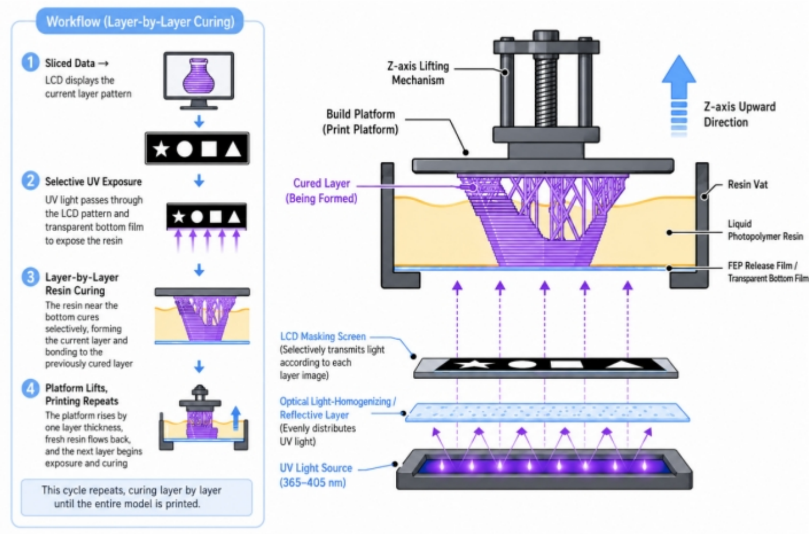

Fig.7. The printing principle and process of MLSA

Compared with point-scanning or line-scanning additive manufacturing techniques, MSLA employs a mask-based area-exposure strategy, enabling the entire cross-section of a layer to be cured simultaneously during a single exposure. Consequently, the fabrication efficiency is significantly improved. Furthermore, the pixel-level exposure control provided by the LCD masking system ensures excellent dimensional accuracy and surface quality for the complex gradient truncated-cone resonators, thereby satisfying the stringent microstructural precision requirements of terahertz absorber fabrication.

After the printing process was completed, residual uncured resin remained attached to the surface of the fabricated samples. Therefore, post-processing procedures were required to improve the sample quality and structural stability. First, the printed samples were immersed in anhydrous ethanol and cleaned using ultrasonic agitation to remove residual resin from the surface and from the narrow gaps within the structure. After cleaning, the samples were allowed to dry naturally under ambient conditions.

Subsequently, the samples were placed in a UV curing chamber for a secondary curing process. This post-curing treatment further activated the unreacted functional groups within the resin, increasing the degree of cross-linking and thereby enhancing the mechanical strength and dimensional stability of the fabricated structures. In addition, the secondary curing process helped reduce internal defects that may have been introduced during the printing procedure.

After the post-curing treatment, the support structures were carefully removed using tweezers and precision tools, and the sample edges were appropriately trimmed and finished. Through the above fabrication and post-processing procedures, the final all-dielectric absorber samples were successfully obtained for subsequent terahertz characterization and performance evaluation.

B.Verification

To obtain the electromagnetic parameters of the high-loss ceramic-filled resin in the terahertz frequency range and establish an accurate material model for subsequent absorber simulations, a terahertz time-domain spectroscopy (THz-TDS) system was employed for material characterization.

Prior to the measurements, flat resin samples with a thickness of 1 mm were fabricated using the MSLA photocuring 3D printing technique. After printing, the samples were cleaned with anhydrous ethanol and subsequently subjected to UV post-curing treatment to ensure sufficient cross-linking of the resin matrix and to achieve good dimensional stability. The electromagnetic properties of the samples were then characterized using a transmission-mode THz-TDS system.

THz-TDS is a non-contact characterization technique capable of simultaneously acquiring both amplitude and phase information of terahertz waves. Owing to its high accuracy and broadband measurement capability, it has been widely applied in dielectric-property characterization and terahertz device evaluation. As illustrated in Fig. 8, the THz-TDS system mainly consists of a femtosecond laser source, a beam-splitting module, a terahertz emitter, a mechanical delay line, a sample measurement region, and a terahertz detector.

During the measurement process, the femtosecond laser pulse is divided into pump and probe beams by the beam-splitting system. The pump beam is directed to the transmitter, where it excites a photoconductive antenna to generate broadband terahertz pulses. The emitted terahertz waves are subsequently collimated and transmitted through the sample under test. Meanwhile, the probe beam is directed to the receiver. By adjusting the optical path difference through the mechanical delay line, the temporal evolution of the terahertz electric field can be sampled point by point, thereby reconstructing the complete terahertz time-domain waveform.

By performing Fourier transformation on the measured time-domain signals, the corresponding frequency-domain spectra can be obtained. Combining the reference signal and sample signal enables the extraction of the complex refractive index, dielectric constant, and loss tangent of the material over the terahertz frequency range, providing reliable electromagnetic parameters for the subsequent simulation and analysis of the proposed absorber.

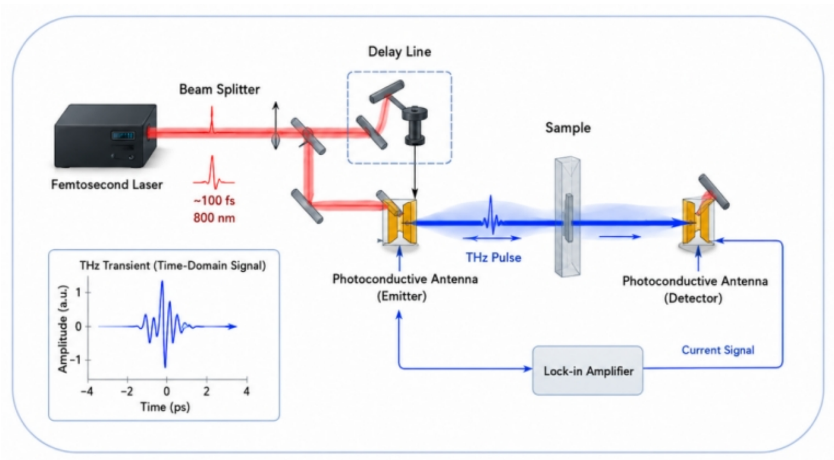

Fig. 8.THz-TDS system

In the measurements, a reference signal was first recorded in the absence of the sample, followed by the acquisition of the transmitted signal through the sample. As terahertz waves undergo amplitude attenuation and phase delay during propagation within the material, the differences between the reference and sample signals contain information regarding the refractive and absorptive properties of the material. By performing a Fast Fourier Transform (FFT) on the acquired time-domain signals, the corresponding frequency-domain amplitude and phase spectra can be obtained. Combined with the known sample thickness, these data enable the retrieval of the refractive index and absorption coefficient of the material over the measured frequency range.

The refractive index characterizes the ability of the material to modulate the propagation velocity of electromagnetic waves, whereas the absorption coefficient quantifies the attenuation of electromagnetic energy within the material. To further determine the complex permittivity of the material, the extinction coefficient, (k), must first be calculated. The relationship between the absorption coefficient and the extinction coefficient is given by：

$$\alpha=\frac{4\pi k}{\lambda} \tag{1}$$

In the formula, α represents the absorption coefficient, k represents the extinction coefficient, and α represents the wavelength of the free space wave.

Since the wavelength of the free space and the frequency satisfy

$$\lambda=\frac{c}{f} \tag{2}$$

Therefore, the expression for the extinction coefficient can be obtained:

$$k=\frac{\alpha c}{4\pi f} \tag{3}$$

Among them, c represents the speed of light in a vacuum, and f represents the frequency of the electromagnetic wave.

The complex refractive index of the material can be constructed using the refractive index n and the extinction coefficient k:

$$\tilde{N}=n-jk \tag{4}$$

According to the theory of electromagnetic wave propagation, the complex refractive index and the complex dielectric constant satisfy the following relationship：

$$\tilde{\varepsilon}_r=(n\text{-}jk)^2 \quad (5)$$

When unfolded, it can yield the real and imaginary parts of the material's complex dielectric constant:

$$\varepsilon'=n^2\text{-}k^2 \quad (6)$$

$$\varepsilon''=2nk \quad (7)$$

Among them, ε' represents the real part of the dielectric constant, reflecting the material's ability to store electromagnetic energy; ε'' represents the imaginary part of the dielectric constant, indicating the level of electromagnetic loss within the material.

To further evaluate the loss characteristics of the material, the loss tangent (Loss Tangent) is commonly used as an important indicator. It is defined as:

$$\tan\delta=\frac{\varepsilon''}{\varepsilon'} \quad (8)$$

The loss tangent characterizes the ability of a material to convert electromagnetic energy into thermal energy. In general, a larger loss tangent corresponds to stronger electromagnetic loss capability, which is beneficial for enhancing the absorption performance of electromagnetic absorbers.

Based on the THz-TDS measurements, the refractive index, absorption coefficient, complex permittivity, and loss tangent of the high-loss ceramic-filled resin were further extracted over the terahertz frequency range. The corresponding results are presented in Fig. 9.

Fig 9(a) illustrates the variation of the absorption coefficient as a function of frequency. It can be observed that the absorption coefficient exhibits an overall increasing trend throughout the frequency range of 0–1.4 THz. This result indicates that the attenuation capability of the material for terahertz waves becomes progressively stronger with increasing frequency, allowing a larger fraction of the incident electromagnetic energy to be dissipated within the material. In particular, the absorption coefficient increases more rapidly above 1 THz, suggesting that the material possesses enhanced electromagnetic loss characteristics in the high-frequency region, which is beneficial for improving the high-frequency absorption performance of the absorber.

Fig. 9(b) presents the frequency-dependent refractive index of the ceramic-filled resin. It can be seen that the refractive index remains within the range of 1.69–1.71 across the entire measured frequency band, exhibiting only slight fluctuations at the lower-frequency region. The overall variation is less than 2%, indicating excellent frequency stability and weak dispersion characteristics in the terahertz regime. Such a stable refractive index is advantageous not only for improving the accuracy of the electromagnetic simulation model but also for maintaining consistent electromagnetic responses over a broad frequency range.

The complex permittivity of the material was subsequently calculated from the extracted refractive index and extinction coefficient. As shown in Fig. 9(c), the real part of the permittivity, ε', remains at a relatively high level throughout the measured frequency range, decreasing gradually from 2.937 at 0.226 THz to 2.836 at 1.353 THz, corresponding to a variation of approximately 3.4%. This result demonstrates that the material possesses strong electric-field energy storage capability and exhibits relatively stable dielectric behavior with respect to frequency. For all-dielectric resonant structures, a stable permittivity is essential for ensuring that different orders of Mie resonances can be excited near their designed frequencies, thereby improving the reliability and predictability of the absorber design.

In contrast, the imaginary part of the permittivity, ε'', exhibits a pronounced increasing trend with frequency. Specifically,ε'' increases from approximately 0.116 at 0.226 THz to 0.327 at 1.353 THz, representing nearly a threefold increase. The increase in ε'' indicates that the intrinsic loss mechanisms of the material become progressively stronger at higher frequencies. As electromagnetic waves propagate through the material, polarization relaxation loss, interfacial polarization loss, and conductive loss collectively contribute to the conversion of electromagnetic energy into thermal energy, thereby enhancing energy dissipation.

Fig.9(d) shows the variation of the loss tangent, tanδ, as a function of frequency. The results reveal that tanδ increases continuously from 0.039 to 0.115 over the measured frequency range. Specifically, the loss tangent is approximately 0.055 at 0.6 THz and increases to about 0.064 at 0.8 THz, before exceeding 0.08 at frequencies above 1 THz. As a measure of the ratio between energy dissipation and energy storage, a larger loss tangent indicates a greater ability of the material to convert electromagnetic energy into heat. Therefore, the observed increase in tanδ confirms that the energy dissipation capability of the material becomes increasingly pronounced with increasing frequency.

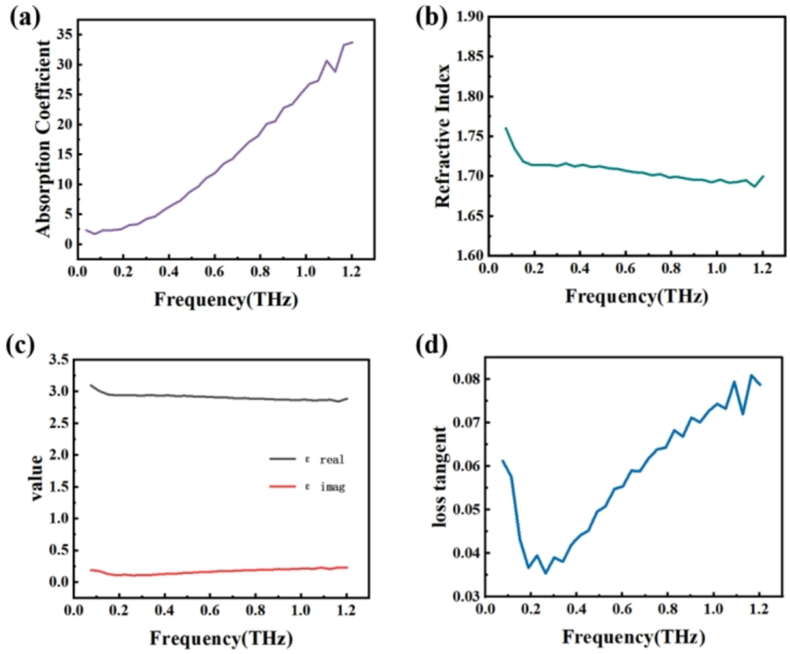

Fig.9. Ceramic resin parameters: (a) absorption coefficient; (b) refractive index; (c) real and imaginary parts of impedance matching; (d) loss tangent

Overall, the results demonstrate that the ceramic-filled resin simultaneously exhibits a stable dielectric constant, weak dispersion characteristics, and continuously enhanced dielectric loss within the frequency range of 0–1.4 THz. The real part of the permittivity remains above 2.8 throughout the measured band, providing effective electromagnetic energy confinement for resonant structures, while the increasing imaginary part of the permittivity and loss tangent ensure efficient energy dissipation. Consequently, the material possesses both energy-storage and energy-dissipation capabilities, making it an excellent candidate for all-dielectric terahertz absorbers and providing a solid material foundation for the realization of broadband and high-efficiency electromagnetic absorption.

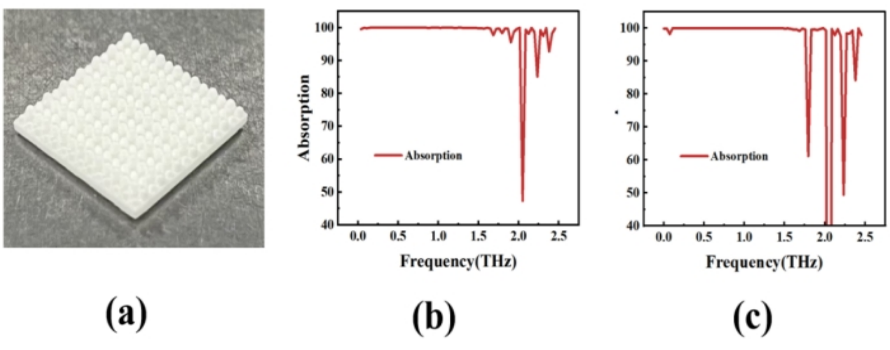

Fig.10. Measured results of the absorber sample: (a) photograph; (b) absorption rate in TE mode; (c) absorption rate in TM mode

To verify the practical absorption performance of the proposed all-dielectric terahertz absorber, absorber samples were fabricated using the MSLA photocuring 3D printing technique. A photograph of the fabricated sample is shown in Fig. 10(a). As can be observed, the fabricated structure exhibits excellent integrity, and the gradient truncated-cone resonators with different dimensions are uniformly distributed across the sample surface. These results demonstrate that the MSLA printing technique is capable of accurately fabricating complex three-dimensional metamaterial structures with high structural fidelity and dimensional consistency.

Based on the measured reflection spectra, the absorptance of the fabricated absorber under different polarization conditions was subsequently calculated. The corresponding results are presented in Figs. 10(b) and 10(c), respectively. Since a metallic ground plane is incorporated beneath the absorber, the transmission can be considered negligible over the measured frequency range. Therefore, the absorption performance of the absorber can be directly evaluated from the measured reflection characteristics.

As shown in Fig. 10(b), under TE-polarized incidence, the absorber maintains a high absorption level over the frequency range of 0–1.8 THz. The absorptance remains close to 100% throughout most of the measured band, with only a few narrow absorption dips appearing above 2 THz. In particular, the minimum absorptance occurs near 2.05 THz. However, within the target operating frequency range, the absorptance remains above 99%, demonstrating the excellent broadband absorption capability of the proposed structure.

Fig.10(c) presents the measured absorption spectrum under TM-polarized incidence. It can be observed that the overall spectral behavior is highly consistent with that obtained under TE polarization. The absorptance also remains close to 100% over the frequency range of 0.2–1.8 THz, with only several localized absorption dips appearing in the higher-frequency region. The strong agreement between the absorption spectra under TE and TM polarizations indicates that the absorber is insensitive to variations in the polarization direction of the incident electric field, thereby exhibiting excellent polarization stability.

Combined with the simulation results presented in the previous chapter, the experimental measurements show good agreement with the numerical predictions, confirming the effectiveness of the proposed design in achieving broadband and highly efficient terahertz absorption. The results further demonstrate that the high-loss ceramic-filled resin absorber fabricated using MSLA printing technology possesses excellent manufacturability and outstanding broadband absorption performance. These characteristics highlight its considerable potential for applications in terahertz electromagnetic manipulation, sensing, stealth technology, and advanced functional electromagnetic devices.

5. Summary

This thesis focuses on the design and fabrication of broadband absorbers operating in the terahertz frequency range. An all-dielectric metamaterial absorber based on a high-loss ceramic-filled resin is proposed and realized. By combining MSLA photocuring 3D printing technology, systematic investigations involving structural design, electromagnetic simulation, absorption mechanism analysis, material characterization, and experimental validation are carried out. The main conclusions are summarized as follows.

(1) Structural Design

An absorber unit composed of four gradient truncated-cone resonators with different dimensions, a high-loss ceramic-filled resin substrate, and a metallic ground plane is proposed. Through structural parameter optimization, localized Mie resonances are excited by resonators of different sizes within the frequency ranges of 0.22–0.35 THz, 0.32–0.48 THz, 0.45–0.65 THz, and 0.60–0.85 THz, respectively. The spectral overlap and coupling of these resonance modes result in broadband electromagnetic absorption.

(2) Absorption Mechanism

Numerical simulations reveal that the broadband high-efficiency absorption originates from the synergistic effects of multiple physical mechanisms. The gradient truncated-cone structure provides smooth impedance matching between free space and the dielectric medium, thereby reducing interfacial reflections. Multi-scale resonators sequentially excite Mie resonances, leading to effective electromagnetic energy localization. The interaction between displacement currents within the dielectric resonators and induced currents on the metallic ground plane forms closed current loops, which excite magnetic dipole resonances and further improve impedance matching. In addition, Fabry–Perot cavity resonances increase the residence time of electromagnetic waves within the structure, while the localized electromagnetic energy is ultimately dissipated through the dielectric losses of the high-loss ceramic-filled resin. Through the combined action of these mechanisms, the absorber achieves an absorptance exceeding 90% over the frequency range of 0.22–0.85 THz.

(3) Material Characterization

The electromagnetic properties of the MSLA-printed ceramic-filled resin are characterized using a terahertz time-domain spectroscopy (THz-TDS) system. The results show that the refractive index remains stable between 1.69 and 1.71 over the frequency range of 0–1.4 THz, while the real part of the permittivity remains above 2.8. Meanwhile, the loss tangent increases gradually from 0.039 to 0.115 with increasing frequency. These characteristics indicate that the material simultaneously possesses stable electromagnetic energy storage capability and enhanced energy dissipation capability at higher frequencies, making it a promising functional material for terahertz absorber applications.

(4) Experimental Validation

The proposed absorber samples are successfully fabricated using MSLA photocuring 3D printing technology. Experimental measurements demonstrate that the absorber exhibits an absorptance close to 100% over the frequency range of 0.2–1.8 THz. Furthermore, the absorption spectra obtained under different polarization conditions show excellent agreement, indicating outstanding polarization stability. The good consistency between the experimental and simulation results further verifies the reliability of the proposed design methodology and the feasibility of the MSLA fabrication process.

In summary, a broadband all-dielectric terahertz absorber based on a high-loss ceramic-filled resin has been successfully designed, fabricated, and experimentally validated in this work. The proposed absorber features a rational structural design, excellent absorption performance, and practical manufacturability. Moreover, the integration of all-dielectric metamaterial design with MSLA 3D printing technology provides a promising approach for the low-cost and high-precision fabrication of terahertz absorbers. The proposed absorber exhibits considerable potential for applications in terahertz electromagnetic manipulation, stealth technology, wireless communications, and other advanced terahertz functional devices.

References

[1] Z. Zhai, L. Zhang, X. Li, S. Xiao, Optics Communications 431, 199 (2019).

[2] J. B. Pendry, D. Schurig, D. R. Smith, Science 312 (5781), 1780 (2006).

[3] X. Jing, D. Feng, Y. Tian, M. Li, C. Chu, C. Li, Y. He, H. Gan, Z. Hong, Optics Express 28 (24), 35528 (2020).

[4] W. Chen, C. A. Balanis, C. R. Birtcher, IEEE Transactions on Antennas and Propagation 64 (9), 4133 (2016).

[5] Y. Qiu, P. Zhang, Q. Li, M. Qiu, Solar Energy 230, 1165 (2021).

[6] D. Yang, H. Mei, L. Yao, W. Yang, Y. Yao, L. Cheng, L. Zhang, K. G. Dassios, Journal of Materials Chemistry C 9 (36), 12010 (2021).

[7] C. M. Watts, X. Liu, W. J. Padilla, Advanced Materials 24 (23), OP98 (2012).

[8] M. Liu, M. Susli, D. Silva, G. Putrino, H. Kala, S. Fan, M. Cole, L. Faraone, V. P. Wallace, W. J. Padilla, Electro-Optical and Infrared Systems: Technology and Applications XVI, SPIE 11160 (2019).

[9] N. L. Mou, B. Tang, J. Z. Li, Y. Q. Zhang, H. X. Dong, L. Zhang, Materials 14 (19), 5708 (2021).

[10] M. M. Chen, X. X. Yang, Plasmonics 19 (3), 1487 (2024).